Journal Pre-proofs

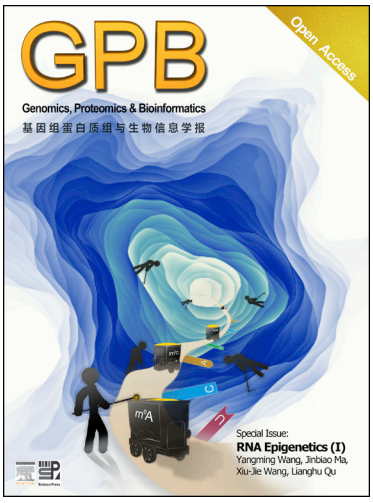

ORIGINAL RESEARCH

RNA Structural Dynamics Modulate EGFR-TKI Resistance Through Controlling *YRDC* Translation in NSCLC Cells

Boyang Shi, Ke An, Yueqin Wang, Yuhan Fei, Caixia Guo, Qiangfeng Cliff Zhang, Yun-Gui Yang, Xin Tian, Quancheng Kan

PII: S1672-0229(22)00142-5
DOI: https://doi.org/10.1016/j.gpb.2022.10.006
Reference: GPB 679

To appear in: *Genomics, Proteomics & Bioinformatics*

Received Date: 30 June 2022
Revised Date: 25 October 2022
Accepted Date: 31 October 2022

Please cite this article as: B. Shi, K. An, Y. Wang, Y. Fei, C. Guo, Q. Cliff Zhang, Y-G. Yang, X. Tian, Q. Kan, RNA Structural Dynamics Modulate EGFR-TKI Resistance Through Controlling *YRDC* Translation in NSCLC Cells, *Genomics, Proteomics & Bioinformatics* (2022), doi: https://doi.org/10.1016/j.gpb.2022.10.006

RNA Structural Dynamics Modulate EGFR-TKI Resistance Through Controlling *YRDC* Translation in NSCLC Cells

Boyang Shi[1,2,3,#], Ke An[1,2,3,#], Yueqin Wang[1,2], Yuhan Fei[4], Caixia Guo[3], Qiangfeng Cliff Zhang[4], Yun-Gui Yang[3,*], Xin Tian[1,2,*], Quancheng Kan[1,2,*]

[1] *Department of Pharmacy, The First Affiliated Hospital of Zhengzhou University, Zhengzhou 450052, China*

[2] *Henan Key Laboratory of Precision Clinical Pharmacy, Zhengzhou University, Zhengzhou 450052, China*

[3] *Key Laboratory of Genomic and Precision Medicine, Collaborative Innovation Center of Genetics and Development, Beijing Institute of Genomics, Chinese Academy of Sciences and China National Center for Bioinformation, Beijing 100101, China*

[4] *MOE Key Laboratory of Bioinformatics, Center for Synthetic and Systems Biology, Beijing Advanced Innovation Center for Structural Biology, Tsinghua-Peking Joint Center for Life Sciences, School of Life Sciences, Tsinghua University, Beijing 100084, China*

[#] Equal contribution.

[*] Corresponding authors.

E-mail: kanqc@zzu.edu.cn (Kan Q), tianx@zzu.edu.cn (Tian X), ygyang@big.ac.cn (Yang YG)

Running title: *Shi B et al / RNA Structural Dynamics Modulate EGFR-TKI Resistance*

The total number of words: 5143.

The total number of figures: 7.

The total number of supplementary figures: 6.

The total number of supplementary table: 2.

The total number of reference: 55.

Abstract

Epidermal growth factor receptor-tyrosine kinase inhibitors (EGFR-TKIs) positively affect the initial control ratio of non-small cell lung cancer (NSCLC). Rapidly acquired resistance to EGFR-TKI is a major hurdle in successful treatment. However, the mechanisms that control the resistance of EGFR-TKI remain largely unknown. RNA structures have widespread and crucial functions in many biological regulations, however, the functions of RNA structures in regulating cancer drug resistance remain unclear. Here, the psoralen analysis of RNA interactions and structures method (PARIS) is used to establish the higher-order RNA structure maps of EGFR-TKI resistant and sensitive cells of NSCLC. Our results show RNA structural regions are enriched in untranslation regions (UTRs) and correlate with translation efficiency (TE). Moreover, *yrdC N*^{6}*-threonylcarbamoyltransferase domain containing* (*YRDC*) promotes resistance to EGFR-TKI. RNA structure formation in *YRDC* 3' UTR suppresses embryonic lethal abnormal vision-like 1 (ELAVL1) binding, leading to EGFR-TKI sensitivity by impairing *YRDC* translation. A potential cancer therapy strategy is provided by using antisense oligonucleotide (ASO) to perturb the interaction between RNA and protein. Our study reveals an unprecedented mechanism through which the RNA structure switch modulates EGFR-TKI resistance by controlling *YRDC* mRNA translation in an ELAVL1-dependent manner.

KEYWORDS: RNA structure; EGFR-TKI resistance; Non-small cell lung cancer; *YRDC*; *ELAVL1*

Introduction

Non-small cell lung cancer (NSCLC) is a primary lung cancer (LC) histological subtype, constituting 85% of all LC cases [1]. Although conventional cytotoxic chemotherapy plays a critical role in treating advanced NSCLC, the latest advancements in individualized medicine have enhanced the responsiveness of oncogenic mutation-harboring NSCLC patients to targeted treatment without inducing severe side effects. Particularly, epidermal growth factor receptor-tyrosine kinase inhibitors (EGFR-TKIs) have been widely studied [2], and *EGFR* genetic mutations are usually present among NSCLC cases (incidence of > 50%) [3]. NSCLC patients containing *EGFR* mutations are sensitive to the first-generation and the second-generation EGFR-TKIs [4,5]. Although disease control and clinical responsiveness rates attained with EGFR-TKI were excellent, resistance soon developed in such cases (mean, 1 year) [6]. Among the various resistance mechanisms of EGFR-TKI, EGFR gatekeeper threonine 790 (T790M) point mutation near the catalytic site has the highest prevalence. EGFR T790M mutation elevates adenosine-triphosphate (ATP) affinity in receptor tyrosine kinase and shows steric hindrance of EGFR-TKI binding, resulting in TKI treatment failure [7]. Although third-generation EGFR-TKI could overcome EGFR T790M resistance, and has been used as the new first-line standard, acquired resistance is inevitable [8], indicating that genetic events are insufficient to explain TKI resistance. Consequently, it is crucial and urgent to identify novel therapeutics or treatments to treat LC with EGFR-TKI resistance.

RNA molecules can fold into complicated structures necessary for the diverse roles and regulation, such as transcription, splicing, polyadenylation, degradation, translation, and localization in cells [9–12]. Recently, combination of chemical probing with high-throughput sequencing methods have been used to study whole-transcriptome secondary structures. Whole-genome RNA secondary structural probing with dimethyl sulfate sequencing (DMS-seq) [13,14], and selective 2'-hydroxyl acylation analyzed by primer extension sequencing (SHAPE-sequencing) [15,16] is conducted in living cells, which revealed the active mRNA structural unfolding, indicating the contribution of

RNA structures to its overall processing. The above approaches indicated significant progress and offered specific data on the single or double stranded RNA regions, but did not detect the direct pairing information between RNA sequences. By using psoralen to crosslink the double stranded RNAs under 365 nm ultraviolet (UV) [17–19], psoralen analysis of RNA interactions and structures (PARIS) could identify the detailed base-pairing regions *in vivo* [20].

Over the past few years, many studies revealed that the widespread regulation of RNA processing, including post-transcriptional regulation in cancer, impacts multiple facets of tumorigenesis and drug resistance [21–23]. Meanwhile, RNA structures are crucial in physiological processes, including embryogenesis [24,25], cardiac specification [26], neurogenesis [27,28], and viral infection [29–33]. Consequently, regulation based on RNA structures is expected to affect tumorigenesis and drug resistance critically. Our study illustrated the *in vivo* RNA structural landscapes in cells with EGFR-TKI resistance and sensitivity using PARIS, and found that the RNA structure switch modulates EGFR-TKI resistance by regulating *yrdC* N^6-*threonylcarbamoyltransferase domain containing* (*YRDC*) mRNA translation in an embryonic lethal abnormal vision-like 1 (ELAVL1)-dependent manner. Collectively, we demonstrate a role of RNA structure-dependent regulation of EGFR-TKI resistance.

Results

Higher-order RNA structure maps of cells with EGFR-TKI resistance and sensitivity

The AZD9291-resistant (AZD9291-R) (**Figure 1**A) and gefitinib-resistant (gefitinib-R) cells (Figure 1B) were established using EGFR-mutant NSCLC cell line (PC9) to explore the mechanisms of RNA structures in LC acquired EGFR-TKI resistance. PARIS assay [20], a high-throughput sequencing methods technology that allows the potent measurement of RNA duplexes in PC9, PC9 (gefitinib-R), or PC9 (AZD9291-R) cells, was performed (Figure 1C). We detected the RNA structures by PARIS method [20] and acquired RNA structural maps (Figure S1A–D; Table S1). Overall,

about 150,000 RNA duplexes from more than 15,000 transcripts were obtained from each of the cell lines (Figure 1D), including intramolecular (Figure S1E) and intermolecular RNA duplexes (Figure S1F). Our study reveals that RNA structures exist in most functional classes of RNAs, including mRNA, miRNA, lncRNA, snoRNA, and snRNA (Figure 1E, Figure S1G and H). Overall, our study constructed RNA structure maps of cells with EGFR-TKI resistance and sensitivity at the transcriptome level.

Having established the RNA structure maps of cells with EGFR-TKI resistance and sensitivity, we performed bioinformatic analysis to investigate the RNA structure's global characteristics. Unlike the previous study which can only identify local structures mainly within the window of < 200 nt, our study identified numerous RNA duplexes (more than 50%) spanning > 200 nt, with more than 30% of them spanning over 1000 nt in cells with EGFR-TKI resistance and sensitivity (**Figure 2**A). To study the RNA structural distribution of mRNA, the two-dimensional heatmaps of enriched RNA structural sites down the mRNA length that aligned transcripts in line with the sites of translation initiation and termination codons were plotted (Figure 2B, Figure S2A and B). Intriguingly, we found that RNA structures were also enriched in untranslation regions (UTRs), translation initiation sites, and stop codons. Except for the local RNA structures, there were many long-range RNA structures across different regions, especially in the UTRs. UTRs are crucial for RNA processing regulation. Thus, RNA structures are the possible regulators for RNA processing modulation in cells with EGFR-TKI resistance and sensitivity.

To explore whether RNA structures are involved in RNA translation, we next performed ribosome profiling (Ribo-seq) and RNA-sequencing (RNA-seq) in PC9, PC9 (AZD9291-R), or PC9 (gefitinib-R) cells (Figure S3A–C). Intriguingly, for structural mRNAs, their translation efficiency (TE) experienced significant impairment compared to non-structural counterparts in these three cell types (Figure S3D). Furthermore, we tested the TE of mRNAs with or without RNA structures, and found that RNA structures impaired TE of mRNA (Figure 2C–E). These results suggest conserved regulation of RNA structure on translation in cells with EGFR-TKI

resistance and sensitivity. To further evaluate RNA structure changes in the transition of EGFR-TKI resistance, the RNA duplexes were compared between cells with EGFR-TKI resistance and sensitivity. Almost 60% of RNA duplexes were conserved between cells with EGFR-TKI resistance and sensitivity (Figure 2F and G), indicating the dynamic RNA structures in the transition of EGFR-TKI resistance. In sum, the RNA structural changes between cells with EGFR-TKI resistance and sensitivity are not found at the whole transcriptome level. Considering that drug resistance turns up from the evolutionary pressure [34,35], we speculate that the changes in RNA structural regulations mainly occur at the transcripts level.

YRDC facilitates LC cell resistance to EGFR-TKI

To determine whether the translation regulation is a crucial regulator for EGFR-TKI resistance, the TE of cells with EGFR-TKI resistance relative to those with EGFR-TKI sensitivity was compared. As a result, EGFR-TKI resistance cause translation changes in both PC9 (gefitinib-R) and PC9 (AZD9291-R) cells compared to PC9 cells (**Figure 3**A). Intriguingly, an 80.1% [1766 / (1766 + 437)] overlap in PC9 (gefitinib-R) and PC9 (AZD9291-R) cells was observed between the upregulated genes in these two EGFR-TKI resistant cells, and 93.7% [6524 / (6524 + 437)] overlap in PC9 (gefitinib-R) and PC9 (AZD9291-R) cells was observed between the downregulated genes (Figure 3A). Hence, the translation regulation between EGFR-TKI resistant and sensitive cells exhibits the similar tendency on TE of these changed genes. Based on the above findings, translation control is speculated to regulate EGFR-TKI resistance. Gene ontology (GO) analysis results revealed that common upregulated genes in EGFR-TKI resistant cells are enriched in processes of intracellular signal transduction, MAPK cascade, Ras protein signal transduction, regulation of Wnt signaling pathway, and small GTPase mediated signal transduction (Figure 3B; Table S2). Common downregulated genes in EGFR-TKI resistant cells are enriched in processes of DNA repair, cell cycle, cellular response to DNA damage stimulus, and response to drug (Figure 3C; Table S2). These results suggested that the translation changes play a crucial role in EGFR-TKI resistance.

Previous studies have reported that *YRDC* regulates RNA translation via involvement in tRNA's N^6-threonylcarbamoyl adenosine (t^6A) synthesis [36–38], and it has been reported that *YRDC* can regulate hepatocellular carcinoma (HCC) cell resistance to lenvatinib by regulating KRAS translation [39]. In our study, we found that *YRDC* has a higher TE in EGFR-TKI resistant cells than EGFR-TKI sensitive cells (Figure 3A). YRDC protein expression was verified through Western blot (Figure 3D). We then investigated the expression of *YRDC* mRNA in the the cancer genome atlas (TCGA) and observed increased *YRDC* expression in NSCLC specimens compared to normal tissue (Figure S4A), indicating its role in tumorigenesis. Thus, we speculate that *YRDC* might be associated with regulating EGFR-TKI resistance in NSCLC cells. The coding sequence (CDS) region of *YRDC* overexpression by plasmid transfection in EGFR-TKI sensitive cells (Figure 3E) was performed to test this hypothesis. Further, a cell counting kit-8 (CCK-8) assay was conducted to detect the cell viability under the treatments of AZD9291 and gefitinib, respectively. *YRDC* overexpression induced a higher EGFR-TKI resistance than the control group in PC9 cells (Figure 3F and G). *YRDC* knockdown by small interfering RNA (siRNA) transfection into EGFR-TKI resistance cells was also performed (Figure 3H). The resistance to EGFR-TKI was impaired under *YRDC* knockdown (Figure 3I and J), indicating that *YRDC* facilitates the resistance to EGFR-TKI in NSCLC cells.

Intriguingly, by analyzing PARIS data, we found that 3' UTR of *YRDC* mRNA forms a double-strand structure only in EGFR-TKI sensitive cells (Fiure S4B), which unwound in both EGFR-TKI resistant cells. Our results have suggested that the RNA structures impair the TE in cells with EGFR-TKI resistance and sensitivity; thus, we speculate that the structural changes may influence the translation of *YRDC* mRNA.

RNA structure in *YRDC* 3' UTR is necessary for EGFR-TKI resistance

For investigating RNA structure's effect on *YRDC* 3' UTR for translation control and EGFR-TKI resistance, four mutants containing endogenous CDS and 3' UTR of *YRDC* with point mutations (Mut-1: U1577C + G1582C, Mut-2: G1585C + G1590U, Mut-3: U1631G + A1636C, Mut-4: C1625A + U1628G) that disrupt base pairing (**Figure 4**A;

Figure S5) were constructed and transfected PC9 cells with the wild type (WT) or mutant *YRDC* plasmids. Only the Mut-1 group showed increased protein expression level (Figure 4B) from the Western blot assay; however, mRNA expression was not changed significantly between WT or mutants (Figure 4C). As a result, RNA structure in *YRDC* 3' UTR impairs the YRDC protein translation instead of the mRNA abundance. Meanwhile, only Mut-1 abolishes this RNA structure's translation inhibition, indicating that the stem formed by 1575–1584 nt and 1629–1638 nt of *YRDC* mRNA was essential for translation control. Furthermore, Mut-1 and Mut-3 can disrupt the base pairing of 1575–1584 nt and 1629–1638 nt of *YRDC* mRNA. However, only Mut-1 (mutant position at 1575–1584 nt of *YRDC* mRNA) abolished the translation inhibition, but not *Mut-3* (mutant position at 1629–1637 nt of *YRDC* mRNA), indicating that the region of 1629–1637 nt is a functional region that modulates translation of *YRDC* mRNA. Instead, the region of 1575–1584 nt may play the role of RNA structural regulator as a flanking sequence. The results of the CCK8 assay also showed that only Mut-1 overexpression induces a higher resistance to EGFR-TKI (Figure 4D and E), supporting that the RNA structure in *YRDC* mRNA 3' UTR possibly has an essential effect on translation control and EGFR-TKI resistance. Antisense oligonucleotide (ASO) was also used to modulate the RNA structure in *YRDC* 3' UTR in EGFR-TKI resistant cells, to test whether this RNA structure can influence EGFR-TKI resistance. ASO was prepared with the phosphorothioate backbone and 2'-*O*-methoxyethyl (2'-MOE) modifications to reduce cell toxicity and enhance nuclease resistance. The results showed that ASO-YRDC (antisense of 1624–1643 nt in *YRDC* mRNA) transfection groups had a lower YRDC protein expression than non-binding ASO (ASO-NC) groups in EGFT-TKIs resistant cells (Figure 4F and G). Besides, the mRNA expression level was not influenced by ASOs transfection (Figure 4H and I). CCK8 assay showed that ASO-YRDC transfection decreased the resistance to EGFR-TKI (Figure 4J and K), suggesting that the RNA structure modulation in EGFR-TKI resistance cells by ASO transfection can restore the sensitivity to EGFR-TKI.

ELAVL1 shows a higher affinity for single-stranded RNA within 3' UTR of *YRDC*

in vitro* and *in vivo

According to previous studies, RNA structures can regulate RNA binding proteins (RBPs) binding to RNA by structural switching [15,24]. Therefore, RNA structure in *YRDC* mRNA 3' UTR might regulate translation by modulating RBPs binding. By analyzing the sequence of 1629–1637 nt of *YRDC* mRNA, we found that this region contains the sequence of UUUAUA, an AU-rich element (ARE). ARE is an important *cis*-element for RNA processing, and previous study have demonstrated that ARE could regulate ELAVL1 binding by RNA structure switch [24]. ELAVL1 is well-known for regulating RNA stability and translation [40]. Thus, we speculated that RNA structure in *YRDC* 3' UTR regulates *YRDC* mRNA translation by controlling ELAVL1 protein binding. Flag-ELAVL1 RNA binding protein immunoprecipitation-quantitative real-time polymerase chain reaction (RIP-qPCR) was performed to test the ELAVL1 binding on *YRDC*. The results showed that ELAVL1 could bind *YRDC* in PC9 (AZD9291-R) and PC9 (gefitinib-R), but not PC9 cells (**Figure 5**A, Figure S6A). To further examine the binding ability of ELAVL1, biotin-labeled RNA pull down assays were conducted using an RNA probe of 1621–1638 nt of *YRDC* mRNA. The results showed that the ELAVL1 can be pulled down by the *YRDC* RNA probe (Figure 5B and C). Similarly, electrophoretic mobility shift assays (EMSA) (Figure S6B) also illustrated that ELAVL1 could bind to the region of 1621–1638 nt of *YRDC* mRNA. Considering the RNA structure switch between cells with EGFR-TKI resistance and those with EGFR-TKI sensitivity, these results suggested that RNA structure in *YRDC* 3' UTR regulates ELAVL1 binding in a structure-dependent manner. To test the role of RNA structure in ELAVL1's binding on 3' UTR of *YRDC* mRNA, RNA probes were synthesized to reconstruct WT RNA structure formed by 1575–1592 nt and 1621–1638 nt of *YRDC* mRNA, rescue and mutant mRNAs with restored and disrupted base pairing within ARE region, respectively (Figure 5D). These assays were repeated by adopting diverse biotin-labeled probe structures. According to RNA pull down (Figure 5E and F) and EMSA (Figure 5G) results, ELAVL1 preferentially binds to 3' UTR of *YRDC* mRNA with single-strand than the double-strand. Overall, the results indicate that the

3' UTR of *YRDC* mRNA could efficiently affect ELAVL1 protein binding by switching the RNA structure between EGFR-TKI resistant and sensitive cells.

RNA structure switch modulates EGFR-TKI resistance by regulating *YRDC* mRNA translation in an ELAVL1-dependent manner

To test the sufficiency of RNA structure in ELAVL1-regulated *YRDC* mRNA translation and EGFR-TKI resistance, *YRDC* reporter mRNAs based on CDS and 3' UTR of *YRDC* with diverse structures (Figure 5D), including the WT where ARE region was base-paired, the mutant disrupting ARE region's base pairing, as well as the rescue restoring base pairing, were constructed. PC9 cells were transfected with WT, mutant, and rescue *YRDC* reporter plasmids under control and *ELAVL1* knockdown condition. Western blot results showed that the mutant group with a single-stranded flanking sequence expressed higher than the WT and rescue groups with the double-stranded flanking sequence. In contrast, no difference was observed after *ELAVL1* knockdown (**Figure 6**A, Figure S6C). The mRNA expression of *YRDC* reporter genes was not influenced under *ELAVL1* knockdown (Figure 6B), indicating that ELAVL1 was not related to *YRDC* mRNA stability. The CCK8 assay also showed that the only mutant reporter genes overexpression induced a higher resistance to EGFR-TKI, and these differences were abolished under *ELAVL1* knockdown (Figure 6C and D). Thus, RNA structure modulates *YRDC* mRNA translation and EGFR-TKI resistance via affecting ELAVL1's accessibility to the ARE region.

Moreover, ASO transfection was performed to test this mechanism. The results showed that ASO-YRDC transfection can impair the expression of YRDC protein, and *ELAVL1* knockdown abolished the difference in YRDC protein levels under ASO-NC or ASO-YRDC transfection (Figure 6E and F, Figure S6D and E). The mRNA expression level in ASO-NC or ASO-YRDC transfection groups was not influenced by *ELAVL1* knockdown (Figure 6G and H). ASO-YRDC transfection also can impair the EGFR-TKI resistance, and *ELAVL1* knockdown also abolished the difference of EGFR-TKI resistance under ASO-NC or ASO-YRDC transfection (Figure 6I and J), consistent with the YRDC protein level. Combined with our previous findings that

RNA structure switch modulates ELAVL1's accessibility to ARE region, these results suggest that ASO can be used to perturb the interaction between RNAs and RBPs, and modulate the EGFR-TKI resistance in NSCLC cells.

In summary, our study put forward one model that depicted the functions of RNA structural alterations in regulating *YRDC* translation and EGFR-TKI resistance by affecting ELAVL1's binding ability to *YRDC* (**Figure 7**).

Discussion

In this study, transcriptome-scale RNA structures were profiled using an acquired resistant model of NSCLC cells that revealed an RNA structure switching-dependent mechanism in regulating EGFR-TKI resistance. Intriguingly, we show that (1) RNA structural regions are enriched in UTR, translation start site, and stop codon, indicating its role of post-transcriptional regulation and translation control, (2) RNA TE are dynamic during the period of drug resistance, and impaired by the RNA structures, and (3) the RNA structure within *YRDC* mRNA's 3' UTR could modulate NSCLC cell translation and EGFR-TKI resistance by regulating ELAVL1 binding. Overall, our study demonstrates RNA structure-based regulation of translation control, which is critical for the drug sensitivity to resistance in NSCLC cells. Furthermore, RNA structures serve as molecular switches for controlling translation in cancer drug resistance, thereby allowing us to overcome drug resistance by modulating RNA structure.

LC is an important factor in cancer-associated death worldwide, while NSCLC is a frequent subtype [1]. Nearly 2/3 of NSCLC cases harbor the carcinogenic driver mutation [41], and the TKI for sensitizing EGFR mutations are investigated widely. Nevertheless, many cases acquired EGFR-TKI resistance in a short time. The mechanisms of resistance are divided into "on-target" and "off-target" [42]. The former occurs in the case of a changed drug's primary target, which limits the target inhibition capacity of the drug, among which the T790M point mutation of EGFR is the most prevalent for gefitinib, erlotinib, or afatinib resistance. Third-generation EGFR-TKI

(AZD9291) solved this problem; however, accompanied by inevitable acquired resistance [8]. The accumulating evidence indicated that the on-target resistance was insufficient to explain the resistance of EGFR-TKI. By contrast, off-target resistance occurs by activating collateral signaling in the downstream signaling or paralleling to the signaling via a driver oncoprotein. Therefore, exploring the new mechanism for overcoming the resistance to EGFR-TKI in LC is crucial for therapy. Our work profiled RNA structures atlas during EGFR-TKI resistance in NSCLC cells, which provided a new perspective that RNA structural switch-mediated translation control modulates drug resistance. Meanwhile, this study used gefitinib and AZD9291 (the first- and third-generation EGFR-TKIs, respectively) for drug resistant-cells construction to obtain the comprehensive RNA structure atlases and general regulation mechanism of EGFR-TKI resistance.

RNA structures are involved in almost all RNA processing, such as polyadenylation, splicing, localization, degradation, and translation [9]. Moreover, recent studies proved that RNA structures are crucial in physiological processes, including embryogenesis [24,25,43], cardiac specification [26], neurogenesis [27], and viral infection [29–33]. Although RNA structures are related to RNA processing and essential for RNA functions, gene regulation based on RNA structure in cancer drug resistance remains unknown. RNA structure is highly dynamic *in vivo*, and is influenced by many factors such as cellular energy state, temperature, RNA helicases, chaperone proteins, and other RBPs [11]. We think there are other regulatory mechanisms promote RNA structural switch in drug resistantance, especially for the protein-directed RNA switch. This work constructed an RNA structure atlas in NSCLC cells, associating RNA structure with post-transcriptional regulation. Firstly, RNA structures were found enriched in UTRs. Previous studies have reported that 35% of conserved structured elements was in UTRs [12], indicating that the RNA structures in UTRs are crucial for RNA fate determination and function. Secondly, RNA structures were found to impair TE in NSCLC cells. RNAs that had more structure within 5' UTR decreased the binding affinity of ribosomes, lowering TE [12]. Meanwhile, ribosomes have an essential effect on unlocking secondary structures in CDS [12,24,25]. Additionally, RNAs double-

stranded structures in 3' UTR impaired translation, possibly due to their higher accessibility to RNA decomposition and translation inhibition mechanisms [9].

YRDC is involved primarily in adenosine N^6-threonyl-carbamoylation in ANN-type tRNA synthesis for recognizing ANN codons [36]. t^6A represents the widely distributed modification necessary to maintain the accurate and efficient translation [37,38], and *YRDC* regulates HCC cell resistance to lenvatinib by regulating *KRAS* translation [39]. The present work found that *YRDC* facilitates EGFR-TKI resistance in NSCLC cells, and the RNA structure in 3' UTR of *YRDC* mRNA can modulate TE, which only exists in PC9 cells that is sensitive to EGFR-TKI. Further studies found that RNA structure reduces the binding affinity of ELAVL1 and impairs the *YRDC* translation. ELAVL1 is crucial for mRNA stability and translation control [40] by binding the AU-rich motifs [44]. Many studies revealed the involvement of ELAVL1 in post-transcriptional regulation of several specific cancers [45,46]. Moreover, the RNA structure greatly affects the binding affinity of its zebrafish ortholog Elavl1a to the AU-rich motif and is essential for zebrafish embryogenesis [24]. Our study performed RNA pull down assays *in vivo* and *in vitro* using structural mutant and rescue form of 3' UTR of *YRDC*. The results showed that ELAVL1 protein preferentially binds to single-strand RNA of 3' UTR of *YRDC*, concordant with the result of the EMSA assay. Moreover, we found that the RNA structural switch in 3' UTR of *YRDC* modulates ELAVL1 binding, essential for controlling *YRDC* translation.

Previous studies reported several mechanisms that regulate translational modulation for shaping tumor development and treatment resistance [47]. The translation modulation by RNA structure reconstruction can be exploited in cancer treatment. Due to the progression of medicinal chemistry, targeted delivery, and molecular mechanisms, ASOs have substantially improved efficacy and properties [48] . Besides inducing target RNA degradation, ASO can also modulate splicing, translation, polyadenylation, *etc*. [48,49]. A recent study showed that ASO could disturb the RBP–RNA target interactions by reconstructing RNA structure [29]. In our study, we found the ASO transfection could decrease the *YRDC* translation and resistance to EGFR-TKI,

indicating that the ASO-mediated RNA structural switch serves as a possible way for overcoming drug resistance in cancer.

Our study establishes RNA structural atlas in EGFR-TKI resistance model, and uses this information to explore the potential RNA structure-dependent mechanism in drug resistance. There are some limitations in this study. First, the RNA structural atlas was obtained from the cellular models with EGFR-TKI resistance and sensitivity that were constructed by using a representative NSCLC cell line, PC9. The LC was highly heterogeneous between different people, although we used two EGFR-TKI resistant cell lines to profile RNA structures, so it was still difficult to represent the RNA structures in all LC cells. Second, although we have demonstrated that the RNA structure-dependent mechanism in drug resistance and potential ASO treatment in different cells, the mechanisms and the action of ASO should be studied further with animal models.

Collectively, our study profiles the RNA structure landscape in cells with EGFR-TKI resistance and sensitivity, and reveals the novel RNA structure switching-dependent mechanism in regulating EGFR-TKI resistance. Notably, the usage of ASO in perturbing the interaction between RNA and protein provide a potential strategy for cancer therapy. Thus, we reasonably speculate that the RNA structure-dependent mechanism and RNA structure targeted drugs could be used for treatment of NSCLC.

Materials and methods

Cell lines and culture conditions

PC9 cells was newly purchased from American Type Culture Collection (ATCC). PC9 (gefitinib-R) and PC9 (AZD9291-R) cells were passaged with low concentration (0.1 μM) of gefitinib (Catalog No. ZD1839, Selleck, Shanghai, China) or AZD9291 (Catalog No. S7297, Selleck, Shanghai, China) and sequentially cultured in increasing concentrations of these TKIs. Cell lines were grown in Roswell Park Memorial Institute (RPMI)-1640 (Catalog No. 11875093, Gibco, Carlsbad, CA) supplemented with 10% fetal bovine serum (Catalog No. 16140078, Gibco, Carlsbad, CA) and

Antibiotic-Antimycotic (Catalog No. 15240062, Gibco, Carlsbad, CA) at 37 °C under 5% CO_2.

PARIS assay

PARIS experiments were performed as previously reported [20]. PC9, PC9 (gefitinib-R), and PC9 (AZD9291-R) cells were treated with AMT (Catalog No. A4330, Sigma-Aldrich, Saint Louis, MO) and crosslinked by 365 nm UV. The lysates were treated by S1 nuclease (Catalog No. EN0321, Thermo Scientific, Carlsbad, MA) and purified by TRIzol (Catalog No. 15596026, Invitrogen, Carlsbad, MA). Purified RNA was treated with ShortCut RNase III (Catalog No. M0245L, NEB, Ipswich, MA). RNA was separated by 12% native polyacrylamide gel and then electrophoresed in a two-dimension 20% urea-denatured gel. Crosslinked RNA proximity ligated with T4 RNA ligase I (Catalog No. M0204L, NEB, Ipswich, MA) and reversed crosslinking with 254 nm UV. The RNA molecules were used for library construction by smRNA-Seq kit (Catalog No. 635031, Clontech, San Jose, CA).

Western blot

Western blot was performed as previously reported [50] and using these antibodies: monoclonal anti-HuR antibody (Catalog No. 390600, Invitrogen, Carlsbad, MA), anti-YRDC antibody (Catalog No. sc-390477, SANTA CRUZ, Dallas, TX), anti-β-Actin antibody (Catalog No. 4967, Cell Signaling Technology, Wuhan, China), and anti-Flag antibody (Catalog No. F7425, Sigma-Aldrich, Saint Louis, MO).

Protein purification

HEK293 were transfected by Flag-tagged *ELAVL1* plasmids using the Polyethylenimine (PEI) (Catalog No. BMS1003, Invitrogen, Carlsbad, MA). Cells were lysed with lysis buffer after 48 h and sonicated for 1 min. The cell debris was removed by centrifugation at 13,300 rpm for 10 min, and the lysates were incubated with the anti-Flag M2 Affinity Gel (Catalog No. A2220, Sigma-Aldrich, Saint Louis, MO) at 4 °C for 4 h. Afterwards the samples were washed five times with lysis buffer

and twice with Tris-buffered saline (TBS) (Catalog No. T5912-1L, Sigma-Aldrich, Saint Louis, MO) buffer. The proteins were eluted by 3× Flag peptide at 4 °C and concentrated by Vivaspin (Catalog No. VS0291, vivaproducts, Littleton, MA).

RNA-seq

Total RNA was isolated from cells by TRIzol reagent. RNA HyperPrep kit (Catalog No. KK8540, KAPA, Saint Louis, MO) was used for RNA-seq library construction.

Ribo-seq

Ribo-seq was performed as previously reported [51] . Cells were incubated in 0.1 mg/ml medium for 5 min at 37℃ and then transferred into 200 μl lysis buffer. After triturating ten times by a 26-G needle, the lysate was centrifugated for 15 min at 20,000 g at 4 °C. 1 μl of RNase I was added to the lysate and incubated at room temperature for 45 min. The lysate was loaded on the MicroSpin S-400 columns (Catalog No. 27-5140-01, GE, Marlborough, MA) and eluted by centrifugation. RNA was extracted from the flow-through using Trizol. Purified RNAs were separated by 15% urea-polyacrylamide gel electrophoresis (PAGE) gel. RNA fragments (27 nt to 30 nt) were recovered and used for library preparation by SMARTer smRNA-Seq kit (Catalog No. 635031, Clontech, San Jose, CA).

Real-time quantitative polymerase chain reaction (RT-qPCR)

RT-qPCR was performed with the SYBR Premix Ex Taq (Catalog No. DRR420A, TAKARA, Shiga, Japan) using CFX96 Real-Time PCR System (Catalog No. 1845096, BIO-RAD, Hercules, CA). The primers are listed as follows, *YRDC*-F: GCCTCTTGTAGGCATTCGGA and *YRDC*-R: AGTACTTTCCAGGGCACAGC.

RNA pull down assay

In vivo or *in vitro* RNA pull down assays were performed by cells extracts or purified proteins as previously reported [24]. In brief, the annealing biotin-labeled RNAs were incubated with cells extracts or purified ELAVL1 proteins for 2 h at 4 °C together with

streptavidin magnetic beads (Catalog No. S1420S, NEB, Ipswich, MA). The beads-bound proteins were eluted in NuPAGE™ LDS buffer (Catalog No. NP0008, Invitrogen, Carlsbad, MA) and detected by Western blot.

EMSA

EMSA assay was performed as previously reported [24]. Purified ELAVL1 proteins were diluted to different concentrations in binding buffer. RNA probes and different concentration purified protein were mixed, and incubated for 30 min at room temperature. The RNA–protein mixture was added with Tris-Borate-EDTA buffer (TBE) sample buffer (Catalog No. LC6678, Invitrogen, Carlsbad, MA) and separated on 10% TBE gel (Catalog No. EC62752BOX, Invitrogen, Carlsbad, MA). The TBE gel was detected by Typhoon 9400 (Catalog No. 29187191, GE Healthcare, Boston, MA). ImageJ was used for quantification. Probe binding ratio was calculated by [RNA–protein / (free RNA + RNA–protein)].

siRNA and ASO transfection

ASO-YRDC: 5'-/i2MOErC/*/i2MOErC/*/i2MOErC/*/i2MOErT//i2MOErG//i2MOErG//i2MOErC//i2MOErT//i2MOErA//i2MOErT//i2MOErA//i2MOErA//i2MOErA//i2MOErG//i2MOErG//i2MOErA//i2MOErT/*/i2MOErA/-3' and ASO-NC: 5'-/i2MOErA/*/i2MOErT/*/i2MOErG/*/i2MOErT//i2MOErG//i2MOErT//i2MOErC//i2MOErC//i2MOErT//i2MOErG//i2MOErT//i2MOErT//i2MOErA//i2MOErA//i2MOErC//i2MOErT//i2MOErC//i2MOErA/*/i2MOErT/*/i2MOErC/*/i2MOErA/-3' were synthesized by Genscript (Nanjing, China). siRNA targeting *ELAVL1* (AAGAGGCAAUUACCAGUUUCA) and *YRDC* (CAUUCGGAUUCCUGAUCAU) were synthesized by Genscript (Nanjing, China). siRNAs and ASOs were transfected by using Lipofectamine RNAiMAX (Catalog No. 13778030, Life technologies, Carlsbad, MA) and used for drug treatment after 24 h.

CCK8 assay

Cell viability was detected by a CCK-8 Cell Counting Kit (Catalog No. A311-02, Vazyme, Nanjing, China) and calculated by GraphPad Prism.

ELAVL1 RIP-qPCR

PC9, PC9 (gefitinib-R), and PC9 (AZD9291-R) cells were transfected with Flag-tagged *ELAVL1* plasmids using the Lipofectamine™ 3000 (Catalog No. L3000015, Life technologies, Carlsbad, MA). And cells were harvested after 48 h and lysed in lysis buffer. Lysates were incubated with Anti-FLAG M2 Magnetic Beads (Catalog No. M8823, Merck, Saint Louis, MO) at 4 °C for 4 h. After washing 3 times, lysates were incubated by proteinase K at 37 °C for 20 min. RNA was purified by Trizol and used for RT-qPCR detection.

RNA-seq data analysis

The raw data was treated using FastQC. Low quality reads and shorter reads were trimmed by cutadapt (V 3.0) and Trimmomatic (V 0.39) [52]. Filtered reads were mapped to the human genome (GRCh38) using Hisat2 (V 2.2.1) with "-p -N -dta". The HTSeq software was used to count reads mapped to each Ensembl gene. The fold change was calculated using the DEseq2 (V 1.26.0) package.

Ribo-seq data analysis

The raw data was evaluated using FastQC. Low quality reads were screened by cutadapt (V 3.0) [53] and Trimmomatic (V 0.39). Screened reads were mapped to the human rRNA transcriptome using Bowtie (v 1.3.0) [54] and unmapped reads were retained for further analysis. The retained reads were mapped to human genome (GRCh38) using Bowtie (v 1.3.0). The mRNAs expression levels were calculated by Cufflinks (v2.2.1). TE was calculated by (fragments per kilobase per million (FPKM) of Ribo-seq) / (FPKM of RNA-seq). For replicated sample, we used the mean expression value.

PARIS data processing and analysis

The raw data was evaluated using FastQC. The low quality reads and shorter reads were screened by cutadapt (V 3.0) and Trimmomatic (V 0.39). Other reads were mapped to human genome (GRCh38) from the Ensembl annotation using STAR (V 2.5.3) with "--outReadsUnmapped Fastx --outFilterMultimapNmax 10 --outSAMattributes All --alignIntronMin 1 --outSAMmultNmax 2 --chimOutType WithinBAM SoftClip --outSAMtype BAM Unsorted --scoreGapNoncan -4 --scoreGapATAC -4 --chimSegmentMin 15 --limitOutSJcollapsed 9000000 --limitIObufferSize 950000000 --chimJunctionOverhangMin 15 --runThreadN 32". The sam file was converted to bam file using SAMtools (V1.11). The gap regions and duplex group were classified by icSHAPE-pipe.

Statistical analysis

Statistical analysis was performed with GraphPad Prism 6.0, and the statistics were analyzed by unpaired Student's *t*-test. *P* values were provided as *, $P < 0.05$, **, $P < 0.01$, and ***, $P < 0.001$.

Data availability

The PARIS, ribo-seq, and RNA-seq raw data have been deposited in the Genome Sequence Archive [55] at the National Genomics Data Center, Beijing Institute of Genomics, Chinese Academy of Sciences / China National Center for Bioinformation (GSA: HRA002235), and are publicly accessible at https://ngdc.cncb.ac.cn/gsa-human.

CRediT author statement

Boyang Shi: Conceptualization, Methodology, Formal Analysis, Data Curation, Validation, Investigation, Writing - original draft, Writing - review & editing. **Ke An:** Formal Analysis, Data Curation, Writing - original draft,Writing - review & editing. **Yueqin Wang:** Methodology, Resources. **Yuhan Fei:** Formal Analysis. **Caixia Guo:** Methodology, Writing - review & editing. **Qiangfeng Cliff Zhang:** Formal Analysis. **Yun-Gui Yang:** Conceptualization, Supervision, Funding Acquisition, Project

Administration, Writing - review & editing. **Xin Tian:** Conceptualization, Supervision, Funding Acquisition, Project Administration, Writing - review & editing. **Quancheng Kan:** Conceptualization, Supervision, Funding Acquisition, Project Administration, Writing - review & editing. All the authors have read and approved the final manuscript.

Competing interests

The authors have declared no competing interests.

Acknowledgments

This work was supported by grants from the Province and Ministry Coconstruction Major Program of Medical Science and Technique Foundation of Henan Province (Grant No. SBGJ202001007), the National Natural Science Foundation of China (Grant Nos. 31870809 and 32121001), and the Special Fund for Young and Middle School Leaders of Henan Health Commission (Grant No. HNSWJW-2020017).

ORCID

0000-0002-5454-4711 (Boyang Shi)

0000-0002-3328-5802 (Ke An)

0000-0003-0408-6721 (Yueqin Wang)

0000-0002-7458-8180 (Yuhan Fei)

0000-0002-2820-705X (Caixia Guo)

0000-0002-4913-0338 (Qiangfeng Cliff Zhang)

0000-0002-2821-8541 (Yun-Gui Yang)

0000-0003-0392-6362 (Xin Tian)

0000-0002-2998-4918 (Quancheng Kan)

References

[1] Siegel RL, Miller KD, Fuchs HE, Jemal A. Cancer statistics 2021. CA Cancer J Clin 2021;71:7–33.

[2] Hirsch FR, Scagliotti GV, Mulshine JL, Kwon R, Curran Jr WJ, Wu Y-L, et al. Lung cancer: current therapies and new targeted treatments. Lancet 2017;389:299–311.

[3] Shi Y, Au JSK, Thongprasert S, Srinivasan S, Tsai C-M, Khoa MT, et al. A prospective, molecular epidemiology study of EGFR mutations in asian patients with advanced non-small-cell lung cancer of adenocarcinoma histology (PIONEER). J Thorac Oncol 2014;9:154–62.

[4] Wu S, Fu L. Tyrosine kinase inhibitors enhanced the efficacy of conventional chemotherapeutic agent in multidrug resistant cancer cells. Mol Cancer 2018;17:25.

[5] Piotrowska Z, Sequist LV. Treatment of EGFR-mutant lung cancers after progression in patients receiving first-line EGFR tyrosine kinase inhibitors : a review. JAMA Oncol 2016;2:948–54.

[6] Yu HA, Arcila ME, Rekhtman N, Sima CS, Zakowski MF, Pao W, et al. Analysis of tumor specimens at the time of acquired resistance to EGFR-TKI therapy in 155 patients with EGFR-mutant lung cancers. Clin Cancer Res 2013;19:2240–7.

[7] Recondo G, Facchinetti F, Olaussen KA, Besse B, Friboulet L. Making the first move in EGFR-driven or ALK-driven NSCLC: first-generation or next-generation TKI? Nat Rev Clin Oncol 2018;15:694–708.

[8] Sullivan I, Planchard D. Osimertinib in the treatment of patients with epidermal growth factor receptor T790M mutation-positive metastatic non-small cell lung cancer: clinical trial evidence and experience. Ther Adv Respir Dis 2016;10:549–65.

[9] Wang XW, Liu CX, Chen LL, Zhang QC. RNA structure probing uncovers RNA structure-dependent biological functions. Nat Chem Biol 2021;17:755–66.

[10] Ganser LR, Kelly ML, Herschlag D, Al-Hashimi HM. The roles of structural dynamics in the cellular functions of RNAs. Nat Rev Mol Cell Biol 2019;20:474–89.

[11] Lewis CJT, Pan T, Kalsotra A. RNA modifications and structures cooperate to guide RNA–protein interactions. Nat Rev Mol Cell Biol 2017;18:202–10.

[12] Mustoe AM, Busan S, Rice GM, Hajdin CE, Peterson BK, Ruda VM, et al. Pervasive regulatory functions of mRNA structure revealed by high-resolution SHAPE probing. Cell 2018;173:181–95.

[13] Ding Y, Tang Y, Kwok CK, Zhang Y, Bevilacqua PC, Assmann SM. *In vivo* genome-wide profiling of RNA secondary structure reveals novel regulatory features. Nature 2014;505:696–700.

[14] Rouskin S, Zubradt M, Washietl S, Kellis M, Weissman JS. Genome-wide probing of RNA structure reveals active unfolding of mRNA structures *in vivo*. Nature 2014;505:701–5.

[15] Spitale RC, Flynn RA, Zhang QC, Crisalli P, Lee B, Jung J-W, et al. Structural imprints *in vivo* decode RNA regulatory mechanisms. Nature 2015;519:486–90.

[16] Smola MJ, Rice GM, Busan S, Siegfried NA, Weeks KM. Selective 2'-hydroxyl acylation analyzed by primer extension and mutational profiling (SHAPE-MaP) for direct, versatile and accurate RNA structure analysis. Nat Protoc 2015;10:1643–69.

[17] Graveley BR. RNA matchmaking: finding cellular pairing partners. Mol Cell 2016;63:186–9.

[18] Aw JGA, Shen Y, Wilm A, Sun M, Lim XN, Boon KL, et al. *In vivo* mapping of eukaryotic RNA interactomes reveals principles of higher-order organization and regulation. Mol Cell 2016;62:603–17.

[19] Sharma E, Sterne-Weiler T, O'Hanlon D, Blencowe BJ. Global mapping of human RNA–RNA interactions. Mol Cell 2016;62:618–26.

[20] Lu Z, Zhang QC, Lee B, Flynn RA, Smith MA, Robinson JT, et al. RNA duplex map in living cells reveals higher-order transcriptome structure. Cell 2016;165:1267–79.

[21] Goodall GJ, Wickramasinghe VO. RNA in cancer. Nat Rev Cancer 2021;21:22–36.

[22] Delaunay S, Frye M. RNA modifications regulating cell fate in cancer. Nat Cell Biol 2019;21:552–9.

[23] Yan F, Al-Kali A, Zhang Z, Liu J, Pang J, Zhao N, et al. A dynamic N^6-methyladenosine methylome regulates intrinsic and acquired resistance to tyrosine kinase inhibitors. Cell Res 2018;28:1062–76.

[24] Shi B, Zhang J, Heng J, Gong J, Zhang T, Li P, et al. RNA structural dynamics regulate early embryogenesis through controlling transcriptome fate and function. Genome Biol 2020;21:120.

[25] Beaudoin J-D, Novoa EM, Vejnar CE, Yartseva V, Takacs CM, Kellis M, et al. Analyses of mRNA structure dynamics identify embryonic gene regulatory programs. Nat Struct Mol Biol 2018;25:677–86.

[26] Xue Z, Hennelly S, Doyle B, Gulati AA, Novikova IV, Sanbonmatsu KY, et al. A G-rich motif in the lncrna braveheart interacts with a zinc-finger transcription factor to specify the cardiovascular lineage. Mol Cell 2016;64:37–50.

[27] Wang J, Zhang T, Yu Z, Tan WT, Wen M, Shen Y, et al. Genome-wide RNA structure changes during human neurogenesis modulate gene regulatory networks. Mol Cell 2021;81:4942–53.

[28] Bernat V, Disney MD. RNA structures as mediators of neurological diseases and as drug targets. Neuron 2015;87:28–46.

[29] Sun L, Li P, Ju X, Rao J, Huang W, Ren L, et al. *In vivo* structural characterization

of the SARS-CoV-2 RNA genome identifies host proteins vulnerable to repurposed drugs. Cell 2021;184:1865–83.

[30] Mizrahi O, Nachshon A, Shitrit A, Gelbart IA, Dobesova M, Brenner S, et al. Virus-induced changes in mRNA secondary structure uncover *cis*-regulatory elements that directly control gene expression. Mol Cell 2018;72:862–74.

[31] Huston NC, Wan H, Strine MS, de Cesaris Araujo Tavares R, Wilen CB, Pyle AM. Comprehensive *in vivo* secondary structure of the SARS-CoV-2 genome reveals novel regulatory motifs and mechanisms. Mol Cell 2021;81:584–98.

[32] Cao C, Cai Z, Xiao X, Rao J, Chen J, Hu N, et al. The architecture of the SARS-CoV-2 RNA genome inside virion. Nat Commun 2021;12:3917.

[33] Ziv O, Price J, Shalamova L, Kamenova T, Goodfellow I, Weber F, et al. The short- and long-range RNA–RNA interactome of SARS-CoV-2. Mol Cell 2020;80:1067–77.

[34] Jamal-Hanjani M, Wilson GA, McGranahan N, Birkbak NJ, Watkins TBK, Veeriah S, et al. Tracking the evolution of non-small cell lung cancer. N Engl J Med 2017;376:2109–21.

[35] Vasan N, Baselga J, Hyman DM. A view on drug resistance in cancer. Nature 2019;575:299–309.

[36] El Yacoubi B, Lyons B, Cruz Y, Reddy R, Nordin B, Agnelli F, et al. The universal YrdC/Sua5 family is required for the formation of threonylcarbamoyladenosine in tRNA. Nucleic Acids Res 2009;37:2894–909.

[37] Murphy FV, Ramakrishnan V, Malkiewicz A, Agris PF. The role of modifications in codon discrimination by tRNA(Lys)UUU. Nat Struct Mol Biol 2004;11:1186–91.

[38] Lescrinier E, Nauwelaerts K, Zanier K, Poesen K, Sattler M, Herdewijn P. The naturally occurring N^6-threonyl adenine in anticodon loop of *Schizosaccharomyces pombe* tRNAi causes formation of a unique U-turn motif. Nucleic Acids Res 2006;34:2878–86.

[39] Guo J, Zhu P, Ye Z, Wang M, Yang H, Huang S, et al. YRDC mediates the resistance of lenvatinib in hepatocarcinoma cells via modulating the translation of KRAS. Front Pharmacol 2021;12:744578.

[40] Hinman MN, Lou H. Diverse molecular functions of Hu proteins. Cell Mol Life Sci 2008;65:3168–81.

[41] Rotow J, Bivona TG. Understanding and targeting resistance mechanisms in NSCLC. Nat Rev Cancer 2017;17:637–58.

[42] McGranahan N, Swanton C. Clonal heterogeneity and tumor evolution: past, present, and the future. Cell 2017;168:613–28.

[43] Shi B, Heng J, Zhou JY, Yang Y, Zhang WY, Koziol MJ, et al. Phase separation of Ddx3xb helicase regulates maternal-to-zygotic transition in zebrafish. Cell Res 2022;32:715–28.

[44] de Silanes IL, Zhan M, Lal A, Yang X, Gorospe M. Identification of a target RNA motif for RNA-binding protein HuR. Proc Natl Acad Sci U S A 2004;101:2987–92.

[45] Abdelmohsen K, Gorospe M. Posttranscriptional regulation of cancer traits by HuR. Wiley Interdiscip Rev RNA 2010;1:214–29.

[46] Schultz CW, Preet R, Dhir T, Dixon DA, Brody JR. Understanding and targeting the disease-related RNA binding protein human antigen R (HuR). Wiley Interdiscip Rev RNA 2020;11:e1581.

[47] Fabbri L, Chakraborty A, Robert C, Vagner S. The plasticity of mRNA translation during cancer progression and therapy resistance. Nat Rev Cancer 2021;21:558–77.

[48] Crooke ST, Baker BF, Crooke RM, Liang X-H. Antisense technology: an overview and prospectus. Nat Rev Drug Discov 2021;20:427–53.

[49] Roberts TC, Langer R, Wood MJA. Advances in oligonucleotide drug delivery. Nat Rev Drug Discov 2020;19:673–94.

[50] Heng J, Lv P, Zhang Y, Cheng X, Wang L, Ma D, et al. Rab5c-mediated endocytic trafficking regulates hematopoietic stem and progenitor cell development via Notch and AKT signaling. PLoS Biol 2020;18:e3000696.

[51] Calviello L, Mukherjee N, Wyler E, Zauber H, Hirsekorn A, Selbach M, et al. Detecting actively translated open reading frames in ribosome profiling data. Nature methods 2016;13:165–70.

[52] Bolger AM, Lohse M, Usadel B. Trimmomatic: a flexible trimmer for Illumina sequence data. Bioinformatics 2014;30:2114–20.

[53] Martin M. Cutadapt removes adapter sequences from high-throughput sequencing reads. EMBnet J 2011;17:10–2.

[54] Langmead B, Trapnell C, Pop M, Salzberg SL. Ultrafast and memory-efficient alignment of short DNA sequences to the human genome. Genome Biol 2009;10:R25.

[55] Chen T, Chen X, Zhang S, Zhu J, Tang B, Wang A, et al. The Genome Sequence Archive family: toward explosive data growth and diverse data types. Genomics Proteomics Bioinformatics 2021;19:578–83.

Figure legends

Figure 1 Comprehensive analysis of RNA structures in EGFR-TKI resistant and sensitive cells

A. CCK-8 assays in PC9 and PC9 (AZD9291-R) cells treated with AZD9291. **B.** CCK-8 assays in PC9 and PC9 (gefitinib-R) cells treated with gefitinib. **C.** Schematic view of *in vivo* RNA structures maps in EGFR-TKI resistant and sensitive cells using PARIS. **D.** The number of RNA–RNA duplexes and transcripts in EGFR-TKI resistant and sensitive cells. **E.** Circos plot of the landscape of RNA–RNA duplexes detected by PARIS in PC9 cells. EGFR-TKI, epidermal growth factor receptor-tyrosine kinase inhibitor; PARIS, psoralen analysis of RNA interactions and structures; CCK-8, cell counting kit-8; UV, Ultraviolet; AMT, 4'-aminomethyltrioxsalen ; RRI, RNA-RNA interaction; mRNA, messenger RNA; miRNA, microRNA; lncRNA, long-noncoding RNA; snoRNA, small nucleolar RNAs; snRNA, small nuclear RNA.

Figure 2 Genome-wide analysis of features in RNA structures in EGFR-TKI resistant and sensitive cells

A. Size distribution of RNA duplexes in transcriptome and genome. Genomic span is the distance between the ends of gapped reads in the genome, while the transcriptomic span excludes introns. **B.** Two-dimensional heatmap showing enrichment of mRNA duplexes based on the location of chimera ends in PC9 cells. **C.** Boxplot chart showing decreased TE for PC9 cells mRNAs displaying RNA structures within UTR or CDS compared to mRNAs without RNA structures. *P* values were calculated by the Wilcox test. **D.** Boxplot chart showing decreased TE for PC9 (AZD9291-R) cells mRNAs displaying RNA structures within UTR or CDS compared to mRNAs without RNA structures. *P* values were calculated by the Wilcox test. **E.** Boxplot chart showing decreased TE for PC9 (gefitinib-R) cells mRNAs displaying RNA structures within UTR or CDS compared to mRNAs without RNA structures. *P* values were calculated by the Wilcox test. **F.** Overlay of RNA duplex groups between PC9 and PC9 (AZD9291-R) cells. **G.** Overlay of RNA duplex groups between PC9 and PC9

(gefitinib-R) cells. TE, translation efficiency; UTR, untranslated region; CDS, coding sequence.

Figure 3 *YRDC* is required for EGFR-TKI resistance

A. Volcano plots showing the $\log_2$ fold changes of TE in PC9 (AZD9291-R) or PC9 (gefitinib-R) cells versus PC9 cells. **B.** Gene enrichment analysis in common upregulated genes compared between EGFR-TKI resistant and sensitive cells. **C.** Gene enrichment analysis in common downregulated genes compared between EGFR-TKI resistant and sensitive cells. **D.** Western blot (left) and statistical (right) analysis show protein level of YRDC in PC9, PC9 (AZD9291-R), and PC9 (gefitinib-R) cells. **E.** Western blot (left) and statistical (right) analysis show protein level of control and *FLAG-YRDC* overexpression in PC9 cells. **F.** CCK-8 assays for PC9 cells transfected with *FLAG-YRDC* expression or control for 24 h followed by AZD9291 treatment for another 48 h. **G.** CCK-8 assays for PC9 cells transfected with *FLAG-YRDC* expression or control for 24 h followed by gefitinib treatment for another 48 h. **H.** Western blot (left) and statistical (right) analysis show protein level of control and *YRDC* knockdown in PC9 (AZD9291-R), and PC9 (gefitinib-R) cells. **I.** CCK-8 assays for PC9 (AZD9291-R) cells with or without *YRDC* knockdown for 24 h followed by AZD9291 treatment for another 48 h. **J.** CCK-8 assays for PC9 (gefitinib-R) with or without *YRDC* knockdown for 24 h followed by gefitinib treatment for another 48 h. ***, $P < 0.001$. Statistical significance was calculated by Student's *t*-test, mean ± SD. *YRDC, yrdC N^6-threonylcarbamoyltransferase domain containing*; SD, standard deviation.

Figure 4 RNA structure in 3' UTR region of *YRDC* contributes to EGFR-TKI resistance via controlling *YRDC* mRNA translation

A. Predicted secondary structure model of the RNA structure in 3' UTR region of *YRDC* mRNA, annotated with genomic coordinates. Red circles represent designs of mutations in the transfection study. **B.** Western blot (left) and statistical (right) analysis show protein level of *FLAG-YRDC* or different *FLAG-YRDC* mutations overexpression

in PC9 cells. **C.** Relative mRNA level of the *FLAG-YRDC* or different *FLAG-YRDC* mutations reporter gene in PC9 cells. **D.** CCK-8 assays for PC9 cells transfected with *FLAG-YRDC* or different *FLAG-YRDC* mutations vectors for 24 h followed by AZD9291 (0.1 μM) treatment for another 48 h. **E.** CCK-8 assays for PC9 cells transfected with *FLAG-YRDC* or different *FLAG-YRDC* mutations vectors for 24 h followed by gefitinib (0.1 μM) treatment for another 48 h. **F.** Western blot (left) and statistical (right) analysis show protein level of YRDC in PC9 (AZD9291-R) cells in control, ASO-NC (non-binding ASO), or ASO-YRDC transfection groups. **G.** Western blot (left) and statistical (right) analysis show protein level of YRDC in PC9 (gefitinib-R) cells in control, ASO-NC (non-binding ASO), or ASO-YRDC transfection groups. **H.** Relative mRNA level of the *YRDC* in PC9 (AZD9291-R) cells in control, ASO-NC (non-binding ASO), or ASO-YRDC transfection groups. **I.** Relative mRNA level of the *YRDC* in PC9 (gefitinib-R) cells in control, ASO-NC (non-binding ASO), or ASO-YRDC transfection groups. **J.** CCK-8 assays for PC9 (AZD9291-R) cells transfected with ASO-NC (non-binding ASO) or ASO-YRDC for 24 h followed by AZD9291 (0.1 μM) treatment for another 48 h. **K.** CCK-8 assays for PC9 (gefitinib-R) cells transfected with ASO-NC (non-binding ASO) or ASO-YRDC for 24 h followed by gefitinib (0.1 μM) treatment for another 48 h. **, $P < 0.01$; ***, $P < 0.001$; n.s., P is not significant. Statistical significance was calculated by Student's *t*-test, mean ± SD. WT, wild type; ASO, antisense oligonucleotide.

Figure 5 ELAVL1 prefers to bind single-stranded RNA in 3' UTR of *YRDC*

A. RIP-qPCR shows the fold enrichment of ELAVL1 binding sites in 3' UTR of *YRDC* mRNA upon Flag pull down in PC9 cells, PC9 (AZD9291-R) cells, and PC9 (gefitinib-R) cells. **B.** Demonstration of endogenous ELAVL1 protein pulled down by RNA probes. **C.** Demonstration of purified Flag-ELAVL1 protein pulled down by RNA probes. **D.** The RNA probes structure prediction models of WT, mutant, and rescue. **E.** Demonstration of ELAVL1 protein pulled down by RNA probes. **F.** Demonstration of Flag-ELAVL1 protein pulled down by RNA probes. **G.** EMSA assay showing the

binding ability of Flag-ELAVL1 protein with WT, mutant, and rescue probes. mean ± SD. **, $P < 0.01$; ***, $P < 0.001$; n.s., P is not significant. Statistical significance was calculated by Student's *t*-test, mean ± SD. RIP-qPCR, RNA binding protein immunoprecipitation-quantitative real-time polymerase chain reaction; EMSA, electrophoretic mobility shift assays; ELAVL1, embryonic lethal abnormal vision-like 1.

Figure 6 RNA structure modulates *YRDC* mRNA translation and EGFR-TKI resistance

A. Western blot (left) and statistical (right) analysis show protein level of the WT, mutant, and rescue FLAG-YRDC upon control and *ELAVL1* knockdown in PC9 cells. **B.** Relative mRNA level of the WT, mutant, and rescue *FLAG-YRDC* reporter gene upon control and *ELAVL1* knockdown in PC9 cells. **C.** CCK-8 assays for PC9 cells transfected with the WT, mutant, and rescue *FLAG-YRDC* upon control and *ELAVL1* knockdown for 24 h followed by AZD9291 (0.1 μM) treatment for another 48 h. **D.** CCK-8 assays for PC9 cells transfected with the WT, mutant, and rescue *FLAG-YRDC* upon control and *ELAVL1* knockdown for 24 h followed by gefitinib (0.1 μM) treatment for another 48 h. **E.** Western blot (left) and statistical (right) analysis show protein level of YRDC in PC9 (AZD9291-R) cells transfected with ASO-NC (non-binding ASO) or ASO-YRDC upon control and *ELAVL1* knockdown. **F.** Western blot (left) and statistical (right) analysis show protein level of YRDC in PC9 (gefitinib-R) cells transfected with ASO-NC (non-binding ASO) or ASO-YRDC upon control and *ELAVL1* knockdown. **G.** Relative mRNA level of the *YRDC* in PC9 (AZD9291-R) cells in control, ASO-NC (non-binding ASO), or ASO-YRDC transfection groups upon control and *ELAVL1* knockdown. **H.** Relative mRNA level of the *YRDC* in PC9 (gefitinib-R) cells in control, ASO-NC (non-binding ASO), or ASO-YRDC transfection groups upon control and *ELAVL1* knockdown. **I.** CCK-8 assays for PC9 (AZD9291-R) cells transfected with ASO-NC (non-binding ASO) or ASO-YRDC upon control and *ELAVL1* knockdown for 24 h followed by AZD9291 (0.1 μM) treatment for another 48 h. **J.** CCK-8 assays for PC9 (gefitinib-R) cells transfected with

ASO-NC (non-binding ASO) or ASO-YRDC upon control and *ELAVL1* knockdown for 24 h followed by gefitinib (0.1 μM) treatment for another 48 h. **, $P < 0.01$; ***, $P < 0.001$, n.s., P is not significant. Statistical significance was calculated by Student's t-test, mean ± SD.

Figure 7 Model showing ELAVL1 regulates *YRDC* mRNA translation in a RNA structure-dependent manner to modulate EGFR-TKI resistance

ARE, AU-rich element.

Supplementary material

Figure S1 Validation of PARIS data quality

A. FPKM correlation of PARIS data between biological replicates for PC9 cells. **B.** FPKM correlation of PARIS data between biological replicates for PC9 (AZD9291-R) cells. **C.** FPKM correlation of PARIS data between biological replicates for PC9 (gefitinib-R) cells. **D.** Overlay of RNA duplex groups between biological replicates. **E.** The number of intermolecular RNA–RNA duplexes and transcripts in EGFR-TKI resistant and sensitive cells. **F.** The number of intramolecular RNA–RNA duplexes and transcripts in EGFR-TKI resistant and sensitive cells. **G.** Circos plot of the landscape of RNA–RNA duplexes detected by PARIS in PC9 (AZD9291-R) cells. **H.** Circos plot of the landscape of RNA–RNA duplexes detected by PARIS in PC9 (gefitinib-R) cells. FPKM, fragments per kilobase per million mapped reads.

Figure S2 RNA structure regions are enriched in UTR, translation initiation sites, and stop codons

A. Heatmap showing the enrichment of mRNA structures in PC9 (AZD9291-R) cells. **B.** Heatmap showing the enrichment of mRNA structures in PC9 (gefitinib-R) cells.

Figure S3 RNA structures correlate with RNA TE

A. FPKM correlation of RNA-seq data between biological replicates. **B.** FPKM

correlation of Ribo-seq data between biological replicates. **C.** Pie chart showing the proportion of Ribo-seq data in three transcripts regions. **D.** Boxplot chart showing decreased TE for mRNAs displaying RNA structures compared to mRNAs without RNA structures. Wilcox test was used for *P* values calculation. Ribo-seq, ribosome profiling; RNA-seq, RNA-sequencing.

Figure S4 RNA structures is associated with *YRDC* translation regulation in EGFR-TKI resistance

A. Expression of *YRDC* in TCGA lung cancer tissues compared to normal tissues. Statistical significance was calculated by Student's *t*-test. **B.** Predicted secondary structure model of the RNA structure in 3' UTR region in PC9 cells based on PARIS data, annotated with genomic coordinates. TCGA, the cancer genome atlas.

Figure S5 Predicted secondary structure model of the RNA structure in 3' UTR of designed mutation (red circles) *YRDC* reporter mRNAs

Figure S6 ELAVL1 protein binds 3' UTR of *YRDC* mRNAs

A. RIP-qPCR shows the fold enrichment of ELAVL1 binding sites in 3' UTR of *YRDC* mRNA upon IgG pull down in PC9, PC9 (AZD9291-R), and PC9 (gefitinib-R) cells. n.s., *P* is not significant. Statistical significance was calculated by Student's *t*-test, mean ± SD. **B.** EMSA showing the binding ability of Flag-ELAVL1 with RNA probes (*YRDC* 1621–1638), mean ± SD. **C.** Western blot demonstrating the absence of ELAVL1 protein upon *siELAVL1* treatment in PC9 cells. **D.** Western blot demonstrating the absence of ELAVL1 protein upon *siELAVL1* treatment in PC9 (AZD9291-R) cells. **E.** Western blot demonstrating the absence of ELAVL1 protein upon *siELAVL1* treatment in PC9 (gefitinib-R) cells. IgG, immunoglobulin G.

Table S1 Summary of PARIS, Ribo-seq, and RNA-seq data

Table S2 GO term enrichment analysis of common changed genes compared between EGFR-TKI resistant cells and EGFR-TKI sensitive cells

CRediT author statement

Boyang Shi: Conceptualization, Methodology, Formal Analysis, Data Curation, Validation, Investigation, Writing - original draft, Writing - review & editing. **Ke An:** Formal Analysis, Data Curation, Writing - original draft,Writing - review & editing. **Yueqin Wang:** Methodology, Resources. **Yuhan Fei:** Formal Analysis. **Caixia Guo:** Methodology, Writing - review & editing. **Qiangfeng Cliff Zhang:** Formal Analysis. **Yun-Gui Yang:** Conceptualization, Supervision, Funding Acquisition, Project Administration, Writing - review & editing. **Xin Tian:** Conceptualization, Supervision, Funding Acquisition, Project Administration, Writing - review & editing. **Quancheng Kan:** Conceptualization, Supervision, Funding Acquisition, Project Administration, Writing - review & editing. All the authors have read and approved the final manuscript.